Molecules during Stellar Formation and Death

Li, X.

Chapter 5

State-selective and thermal rates for $H + OH(v, j) \longrightarrow O + H_2$

Abstract.
The dynamics of the reaction H + OH → O (^{3}P) + H_2 have been studied in a series of quasi-classical trajectory (QCT) calculations and transition state theory (TST) methods using high quality $^3A'$ and $^3A''$ potential energy surfaces (PESs). Accurate OH(v, j) state resolved cross sections and rate constants on both potential energy surfaces are presented and fitted for OH at ($v = 0,\ j = 0 - 16$) and ($v = 1,\ j = 0 - 6$). The cross sections were calculated for different collisional energies (E_c), ranging from the threshold energy at each specific rovibrational state up to 1.0 eV with step sizes of 0.1 eV or less. They increase steeply with collision energy when the barrier to reaction can be overcome, after which the cross sections stay nearly constant with energy. State resolved rate constants in the temperature range 200 – 2500 K are presented based on the cross sections. Total thermal rate constants were calculated by summing the rates for reaction on the $^3A'$ and $^3A''$ potential energy surfaces weighted by 1/3 and taking into account the thermal populations of the rovibrational states of the OH molecules. The current calculated thermal rate constants generally agree well with previous indirectly obtained rate constants by Tsang *et al.* (1986). It is shown that the improved canonical variational transition (CVT) treatments with the approximation of zero-curvature tunneling (ZCT) or small-curvature tunneling (SCT) produce results more in accord with the QCT results than the TST and CVT methods. The reactions are governed by the direct reaction mechanism. The rate constants for OH in excited vibrational and rotational states are orders of magnitude larger than the thermal rate constants, which needs to be taken into account in astrochemical models.

X. Li, C. Arasa, M. C. van Hemert, and E. F. van Dishoeck
J. Phys. Chem. A, **117** , 12889 (2013)

5.1 Introduction

The O (^{3}P) + H_2 system has attracted interest for more than half a century (Garton et al. 2003). In addition to its fundamental significance in chemical dynamics, it is also known to be a participant in combustion processes (Baulch et al. 1992) and plays an important role in warm interstellar gas such as shocks, clouds exposed to intense UV radiation and the inner regions of protoplanetary disks (Graff & Dalgarno 1987; Sternberg & Dalgarno 1995; Agúndez et al. 2008a). Extensive theoretical (Zhai et al. 2012; Han & Zheng 2011; Liu & Shi 2010; Li & Han 2009; Pettey & Wyatt 2008; Weck et al. 2006; Wang et al. 2006; Garashchuk et al. 2006; Atahan et al. 2006; Chu et al. 2005; Braunstein et al. 2004; Brandão et al. 2004; Balakrishnan 2004; Maiti & Schatz 2003; Balakrishnan 2003; Rogers et al. 2000a; Hoffmann & Schatz 2000; Varandas et al. 1997; Chatfield et al. 1993; Joseph et al. 1988; Robie et al. 1987; Schatz 1985; Bowman et al. 1984; Schatz et al. 1981; Walch et al. 1980; Howard et al. 1979; Light 1978) and experimental (Garton et al. 2006), investigations have been carried out to elucidate the dynamics of the O (^{3}P) + H_2 reaction, which has a classical energy barrier of about 0.57 eV (Rogers et al. 2000a) and at low temperatures occurs mainly through tunneling (Robie et al. 1987). Thanks to long-term efforts of constructing and improving the potential energy surfaces (Zhai et al. 2012; Atahan et al. 2006; Brandão et al. 2004; Rogers et al. 2000a; Joseph et al. 1988; Howard et al. 1979), classical and quantum mechanical calculations have been carried out to provide fruitful information on many aspects of this system, such as the kinetics (Westenberg & Haas 1967; Baulch et al. 1994), isotope effects (Sultanov & Balakrishnan 2004), state selective dynamics (Light 1978; Johnson & Winter 1977; Reynard & Donaldson 2001), intersystem crossing (Chu et al. 2005; Robie et al. 1987), nonadiabatic effects (Han & Zheng 2011; Li & Han 2009; Garashchuk et al. 2006), and stereodynamics (Liu & Shi 2010; Wei et al. 2010). Among these PESs, the high quality generalized London-Eyring-Polanyi-Sato (LEPS) double-polynomial (GLDP) surfaces ($^3A'$ and $^3A''$) reported by Rogers et al. (2000a) are widely adopted in scattering simulations and can yield chemically accurate results which are in good agreement with experiments (Garton et al. 2003; Weck et al. 2006; Garton et al. 2006). For example, the reaction cross sections measured by crossed molecular beam experiments are well reproduced by quantum wave packet calculations based on this PES (Garton et al. 2003). Another combined experimental and theoretical investigation on the isotopic substituted reaction O (^{3}P) + D_2 also found good qualitative agreement between the measured dynamic results and the single-surface quasi-classical trajectory calculations (Garton et al. 2003, 2006). These studies also showed that intersystem crossing with the excited singlet states have at most a very minor effect on the reaction probabilities. In fact, according to the exact quantum study of spin-orbit-induced intersystem crossing by Chu *et al.* (Chu et al. 2005, 2006), the effects of spin-orbit coupling on the total reaction cross sections are insignificant if the fine-structure resolved cross sections in the O ($^3P_{2,1,0}$) + H_2 reaction are treated statistically. The quantum scattering calculations performed by Balakrishnan *et al.* (Garashchuk et al. 2006; Balakrishnan 2004, 2003) mainly reported thermal rate coefficients, and found the reaction probability of the $^3A'$ PES to be slightly smaller than that of the $^3A''$ PES in the energy range of 0.5 – 1.2 eV. Brandão et al. (2004) extended the $^3A''$ PES from Rogers et al. (2000a). with van der Waals interactions and used it to study the influence

of the long-range potential on the reaction rates, especially at (ultra) cold temperatures, where tunneling and resonances are significant.

There are far fewer studies of the reverse reaction. The most detailed calculations have focused on the cross sections, thermal rate constants and rate coefficients of the isotope exchange reaction D + OH → OD + H, which plays an important role in interstellar clouds (Atahan et al. 2005; Howard & Smith 1982; Dunne & Murrell 1983; Margitan et al. 1975). However, few studies have been done for the more basic process

$$\mathrm{H}(^2\mathrm{S}) + \mathrm{OH}(^2\Pi)(v,\ j) \underset{k_{-1}}{\overset{k_1}{\rightleftharpoons}} \mathrm{O}(^3\mathrm{P}) + \mathrm{H}_2(^1\Sigma_g^+) \tag{5.1}$$

This is partly because obtaining a beam of OH is experimentally challenging (Radenovic et al. 2003). The rate constant for k_1 in Eq. 5.1 offered in the National Institute of Standards and Technology (NIST) Chemical Kinetics Database (Fernandez-Ramos et al. 2013), which is often employed in astrochemical models but dates from 1986, was derived from the rate constant of the reverse reaction,

$$k_1 = K \,/\, k_{-1} \tag{5.2}$$

where K is the kinetic reactive rate constant. The k_{-1} was suggested according to a combined experimental and TST investigations where the transition state theory (TST) calculations were based on an older PES (Cohen & Westberg 1983). Since the uncertainty of k_1 arises from the uncertainties in both K and k_{-1}, determination of more reliable rate constants for this reaction using a more accurate PES are warranted. Moreover, there is a growing need in astrochemical models for state-specific rate constants in addition to thermal rates (Tappe et al. 2008; Mandell et al. 2012; Salyk et al. 2008; Pontoppidan et al. 2010). Specifically, non-thermal excitation of OH in high rotational and/or vibrational states has been observed in shocks (Tappe et al. 2008) and in the inner regions of protoplanetary disks (Mandell et al. 2012; Salyk et al. 2008; Pontoppidan et al. 2010), which may drive the H + OH reaction. In these regions, gas temperatures are up to 2000 K.

In this chapter, we have carried out the first QCT, TST, and variational transition state theory (VTST) calculations for the title reactions on the $^3A'$ and $^3A''$ GLDP PESs (Rogers et al. 2000a) of OH($v,\ j$) resolved rate constants and thermal rate constants are reported. Other than using the approximate ZCT and SCT methods, tunneling is ignored in the chapter due to the classical nature of the QCT approach. The chapter is organized as follows: in Section 2 we briefly review the theoretical methodologies. In Section 3, results and discussion are presented. Finally, Section 4 closes with the conclusions.

5.2 Chemical models

5.2.1 Potential Energy surface

Scattering calculations were performed on the $^3A'$ and $^3A''$ potential energy surfaces of Rogers et al. (2000a), which are the most accurate published surfaces to date for this reaction. These surfaces, generated from 951 geometries and with high-accuracy for a subset of 112 of these geometries, were based on complete-active-space self-consistent-field (CASSCF) computations using correlation-consistent basis sets. Two different fitting methods, the rotating Morse spline (RMOS) method and the GLDP method, were

employed and compared to each other and also to a previous empirical LEPS surface. Overall, the GLDP fit and RMOS fit to the *ab initio* data are very similar, but the GLDP fit has a higher fitting accuracy and should yield accurate reactive scattering calculations. The GLDP PESs employed in our work consist of two terms:

$$V_{\mathrm{GLDP}} = V_{\mathrm{GLEPS}} + V_{\mathrm{DPOLY}} \tag{5.3}$$

V_{GLEPS} is a Generalized LEPS term and V_{DPOLY} a sum of two high-order polynomials (as functions of the three interatomic distances) multiplied by switching functions. In V_{GLEPS}, a cubic spline fit of near-asymptotic *ab initio* data for each of the three isolated diatomic molecules is used instead of the Morse function of the usual LEPS function. Further details can be found in the original reference (Rogers et al. 2000a).

A typical A + BC reaction can lead to four possible scattering channels: A + BC, AB + C, AC + B, and A + B + C. We have focused on the H + OH → O + H_2 abstraction reaction both on the $^3A'$ and on the $^3A''$ PESs. The two potential energy surfaces have similar characteristics and are degenerate for collinear configurations. Both of them are dominated by a barrier and have a broad van der Waals well along the entrance valley. The barrier heights on the $^3A'$ and $^3A''$ PESs are 0.476 and 0.468 eV, and the depths of the wells are 0.009 and 0.004 eV, respectively. The differences in barrier heights and van der Waals depths in the two PESs are smaller than the root-mean-square (rms) error (±0.0129 eV) induced by the fitting procedure and are in any case not relevant for the temperature range considered here. However, these small differences may be responsible for slightly different reaction thresholds, and also play a role in quantum mechanical studies at low collision energies and stereodynamics studies.

The corresponding energy-level diagram for different rovibrational states $(v,\ j)$ of the OH molecule is shown in Figure 5.1. The rovibrational energy levels $E_{v,j}$ were calculated from the PESs using the QCT code and are presented both with and without the zero-point energies. In practice, the zero-point energy of OH molecule needs to be taken into account for the reactive channel. In our case, j is the purely rotational angular momentum of the OH molecule (often denoted as N in the spectroscopic literature) since in our work electronic orbital and spin angular momenta are discarded. Each OH rotational level j modeled here, is in reality split into two different spin states, $^2\Pi_{1/2}$ and $^2\Pi_{3/2}$, which have an energy difference of only 0.017 eV (Maillard et al. 1976). This difference is ignored in our calculations.

5.2.2 Quasi-classical trajectory calculations

In this work, we have used the Venus96 QCT code developed by Hase et al. (1996) to compute cross sections as functions of energy, from which state-resolved rate constants as well as the thermal rate constants are subsequently calculated. In all cases, the initial parameters are as follows. An initial distance of 6.4 Å is adopted between the attacking H atom and the center of mass of the target OH molecule. Batches of 2×10^4 trajectories have been carried out for each collision energy of the incident hydrogen atom. The integration step size is chosen to be 0.1 fs, which is small enough to ensure the conservation of the total energy and the total angular momentum. To calculate thermal rate constants, for both $^3A'$ and $^3A''$ PESs, the initial rovibrational conditions of the OH molecule were

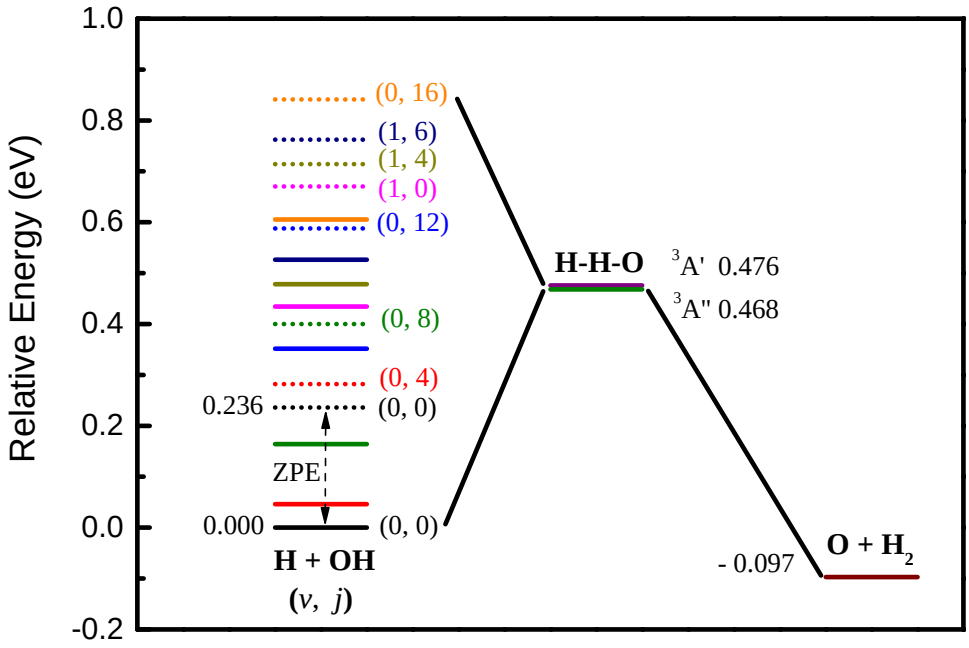

Figure 5.1 — Schematic energy-level diagram for the abstraction reactions H+OH($v,\ j$) $\rightarrow O(^3\mathrm{P}) + \mathrm{H}_2$ at various rovibrational ($v,\ j$) states of OH, in solid lines. Dotted lines: corrected energy levels which include the zero-point vibrational energy (ZPE). For the H + OH channel, this ZPE is taken into account in the QCT calculations.

chosen to include the range of states ($v = 0,\ j = 0 - 16$) and ($v = 1,\ j = 0 - 6$). To evaluate the cross sections, the collision energies (E_c) were set up on a finely spaced grid: on the $^3A'$ PES, for $v = 0$ at $j = 0$ up to 16, E_c were chosen as follows: from 0.2 to 0.32 with a step size of 0.02 eV; 0.35 eV, and from 0.4 to 1.0 eV with a step size of 0.1 eV. For $v = 1$ at $j = 0$ up to 6, E_c were chosen at 0.06, 0.08, 0.10, 0.12, 0.15, 0.2, 0.25, and from 0.3 to 1.0 eV with a step size of 0.1 eV. For the $^3A''$ state, the selected E_c are the same as those on $^3A'$ state except those at $v = 0$ and $j = 7$ up to 16, which employed the same energy values as for $v = 1$, $j = 0$ up to 6 on the $^3A'$ PES.

During the QCT simulations, the impact parameter b is sampled from $0 \leq b \leq b_{\max}$ by $b = b_{\max}\xi_0^{1/2}$, where ξ_0 is a pseudorandom number, and the maximum impact parameter, b_{max}, is the value of b for which the reactive probability drops to zero when $b \geq b_{\max}$. In our work, b_{max} is optimized by trial calculations with a range of b_{max} values at fixed initial condition of the reactants, until the reactive probability of the observed channel is zero while $b = b_{max}$. The criterion is that at most one reactive trajectory occurs among a large sum of total trajectories (for example, 10^4), thus the reaction probability is approximately zero. Generally, 3 – 6 trials are necessary to optimize b_{max} at a fixed E_c. In the present calculations, b_{max} has been determined by running batches of 10^4 trajectories. Overall, the value of b_{max} increases with increasing rovibrational state of the OH reactant at each fixed E_c leading to a corresponding enhancement of the cross section as well as the relevant rate constant. According to our experience, a slightly higher b_{max} does not affect the cross sections much, whereas a too small value will result in significant errors.

The integral cross section, $\sigma(v, j)$, and the associated uncertainties $\Delta\sigma(v,\ j)$ at a

certain rovibrational level $(v,\ j)$ can be determined from (Karplus et al. 1965)

$$\sigma(v,j) = \pi b_{\max}^2 \frac{N_r(v,j)}{N(v,j)},$$
$$\Delta\sigma(v,j) = \sqrt{\frac{N(v,j) - N_r(v,j)}{N(v,j)N_r(v,j)}}\sigma(v,j) \tag{5.4}$$

where N and Nr denote the total number of sampled and reactive trajectories, respectively. Eq. 5.4 is only valid when the $\xi_0^{1/2}$ sampling method is used. Since we have employed a large number of trajectories, the standard error is $\pm 20\%$ for collisional energies near threshold and less than $\pm 6\%$ when the collisional energy is more than 0.4 eV.

Subsequently, the specific rate constant at a temperature T for an initial rovibrational $(v,\ j)$ state of the OH molecule is calculated from the integral cross sections by averaging over a Maxwell distribution of energies through

$$k(T;v,j) = \sqrt{\frac{8k_{\rm B}T}{\pi\mu_R}}(k_{\rm B}T)^{-2}\int_0^{1.0} E_c\sigma(v,j)\exp\left(\frac{-E_c}{k_{\rm B}T}\right)dE_c \tag{5.5}$$

where $k_{\rm B}$ is the Boltzmann constant, μ_R the reduced mass of the reactants, and E_c the collision energy.

The thermal rate constant for an initial vibrational state can be written as

$$k(T) = \sum_{v=0}\sum_{j=0} p_{vj}(T)k(T;v,j) \tag{5.6}$$

where $p_{vj}(T)$ are the fractional population of the OH molecule for a thermal distribution at temperature T, calculated by

$$p_{vj}(T) = (2j+1)\exp\left(-E_{v,j}/k_{\rm B}T\right)/Q_{v,j}(T) \tag{5.7}$$

with

$$Q_j(T) = \sum_{v}^{\infty}\sum_{j=0}^{\infty}(2j+1)\exp\left(-E_{v,j}/k_{\rm B}T\right) \tag{5.8}$$

The fractional populations of the OH molecule as functions of j at various temperatures are shown in Figure 5.2. This figure demonstrates that j levels up to 16 in $v = 0$ indeed need to be included at higher temperatures. In the calculations, the sum of Eq. 5.6 is truncated at $j =$ 16 for $v = 0$ and $j = 6$ for $v = 1$ for both PESs. The rate constants have been calculated by summing the rates on each of the potential energy surfaces ($^3A'$ and $^3A''$) weighted by 1/3 (Schatz 1985; Bowman et al. 1984; Balakrishnan 2003; Walch et al. 1980). This is because the overall reaction leads to 3 triplet potential energy surfaces, 2 having A'' symmetry, and 1 A'. One of the A'' symmetry PESs does not contribute to the reaction since it has a higher energy barrier (Wang et al. 2006). Finally, to make these data available to astronomers in a convenient form, the specific rate constants for individual OH$(v,\ j)$ states were fitted to the Arrhenius form, $k(T) = \alpha \times (T/300)^{\beta} \times e^{(-\gamma/T)}$, where T is the gas temperature, α is known as the pre-exponential factor, β dictates the temperature dependence of the rate coefficient and γ is the activation energy of the reaction in units of K.

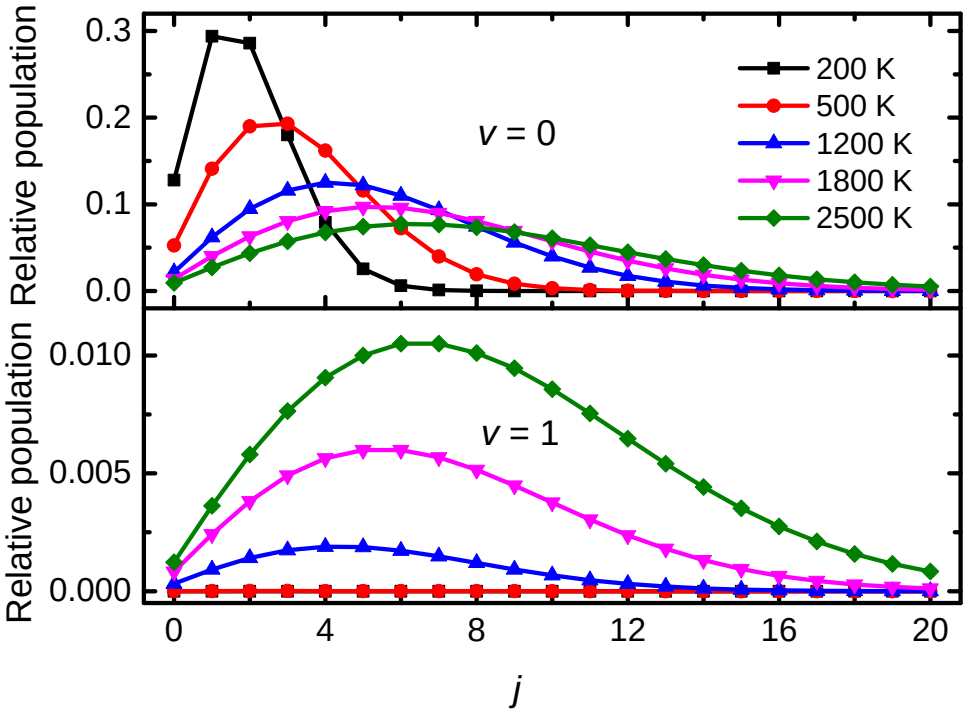

Figure 5.2 — Relative populations of OH $(v,\ j)$ molecules as a function of j for thermal excitation at various temperatures, for $v = 0$ and 1.

5.2.3 Transition state theory

Transition state theory is a useful tool for calculating approximate rate constants for reactions occurring in the gas phase and in the condensed phases based on the barrier height, the density of states at the transition state Q, and on the (products of the) partition functions of the reactants F. The rate constant calculations can be improved by the variational transition state theory (VTST), where a dividing surface is defined so that all reactive trajectories must pass through it. The dividing surface is defined along the reaction coordinate s, which is the distance along the minimum energy path (MEP), with $s = 0$ at the saddle point, negative on the reactant side, and positive on the product side. The rate constants according to the generalized transition state theory (GTST) as a function of temperature T and s (Ju et al. 2009; Truhlar & Garrett 1984) is given by

$$k^{\mathrm{GTST}}(T,s) = \frac{\alpha}{\beta h}\frac{Q^{\mathrm{GTST}}(T,s)}{\Phi^{\mathrm{R}}(T)}e^{-\beta V_{\mathrm{MEP}}(s)} \tag{5.9}$$

where α is the number of symmetry equivalent reaction paths, $\beta = \frac{1}{k_{\mathrm{B}}T}$, and h is Planck's constant. $Q^{\mathrm{GTST}}(T,\ s)$ and $\Phi^{\mathrm{R}}(T)$ are the density of states at the generalized transition state at point s and the partition function of the reactants, respectively. $V_{\mathrm{MEP}}(s)$ is the potential energy at point s along the minimum energy path. The VTST rate constant k^{VTST} is the minimum value of the GTST rate constant (Eq. 5.9) at a given T:

$$k^{\mathrm{VTST}}(T) = \min_s k^{\mathrm{GTST}}(T,s) = k^{\mathrm{GTST}}(T, s^{\mathrm{CVT}}(T)) \tag{5.10}$$

Table 5.1 — Parameters of the fitting formula $\sigma = P_1 \times (1 - (P_2/E_c)^2)^3 \times E_c^{P_3}$ for the cross sections σ (Å^2) as a function of collision energy E_c for various OH($v,\ j$) states on the $^3A'$ and $^3A''$ potential energy surfaces.

	$^3A'$			$^3A''$		
$(v,\ j)$	P_1	P_2	P_3	P_1	P_2	P_3
(0, 0)	0.328	0.215	0.226	0.456	0.235	0.730
(0, 1)	0.358	0.217	0.420	0.446	0.237	0.625
(0, 2)	0.355	0.218	0.610	0.441	0.234	0.637
(0, 3)	0.359	0.225	0.572	0.431	0.234	0.636
(0, 4)	0.380	0.235	0.602	0.437	0.232	0.516
(0, 5)	0.402	0.238	0.638	0.460	0.224	0.631
(0, 6)	0.407	0.236	0.724	0.455	0.212	0.620
(0, 7)	0.426	0.220	0.890	0.463	0.135	1.181
(0, 8)	0.414	0.217	0.676	0.476	0.132	1.010
(0, 9)	0.440	0.203	0.745	0.525	0.129	0.971
(0, 10)	0.482	0.206	0.620	0.592	0.129	0.876
(0, 11)	0.513	0.201	0.590	0.633	0.125	0.772
(0, 12)	0.555	0.196	0.573	0.715	0.123	0.697
(0, 13)	0.613	0.182	0.701	0.715	0.123	0.697
(0, 14)	0.661	0.180	0.630	0.840	0.116	0.473
(0, 15)	0.719	0.183	0.532	0.898	0.108	0.377
(0, 16)	0.747	0.181	0.407	0.959	0.094	0.391
(1, 0)	0.794	0.018	0.172	1.101	0.025	0.317
(1, 1)	0.841	0.034	0.212	1.124	0.026	0.429
(1, 2)	0.859	0.052	0.257	1.042	0.058	0.239
(1, 3)	0.845	0.071	0.211	1.017	0.061	0.254
(1, 4)	0.894	0.074	0.333	1.056	0.062	0.329
(1, 5)	0.960	0.076	0.469	1.077	0.062	0.355
(1, 6)	0.988	0.076	0.547	1.106	0.061	0.341

where $s^{\mathrm{CVT}}(T)$ is the location of the Canonical Variational Transition (CVT) state at a given temperature T. Quantum effects may be important for light systems and at lower temperatures, especially for tunneling along the reaction-coordinate motion. In order to include these effects, the $k^{\mathrm{VTST}}\ (T)$ is multiplied by a transmission coefficient, usually by the approximation of Zero Curvature Tunneling (ZCT) or Small Curvature Tunneling (SCT), see Ju et al. (2009). Here, TST, CVT, CVT/ZCT and CVT/SCT have been employed to calculate the rate constants on the $^3A'$ and $^3A''$ surfaces for the $(v = 0,\ j = 0)$ state of the reactant molecule, yielding the corresponding rate constants in the temperature range of 200 – 2500 K. In all transition state calculations the polyrate program (Fernandez-Ramos et al. 2007) was used.

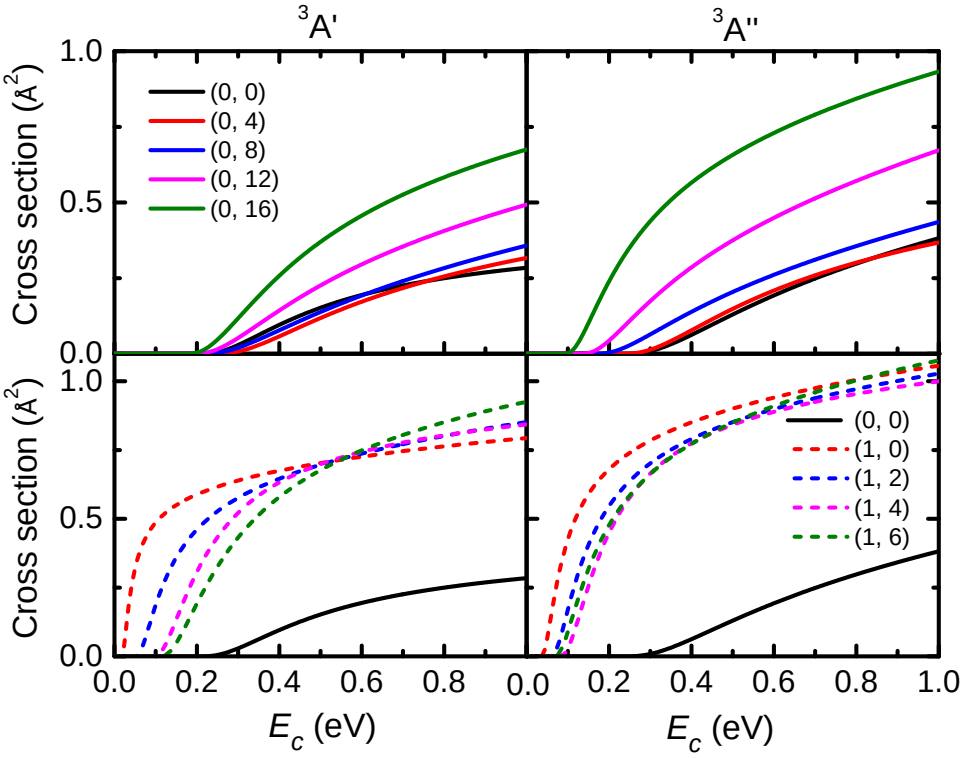

Figure 5.3 — Integral cross sections as functions of collision energy for the title reaction at different rovibrational levels $(v,\ j)$ of OH for the two PESs $^3A'$ and $^3A''$.

5.3 Results and Discussion

5.3.1 Integral cross sections

Cross sections starting from various initial excitation states, $(v,\ j)$, of the OH molecule have been computed to obtain the thermal rate constant for the title reaction. For $^3A'$ and $^3A''$ PESs, integral cross sections for $(v = 0,\ j = 0 - 16)$ and $(v = 1,\ j = 0 - 6)$ have been calculated. All of these cross sections are fitted to the formula $\sigma = P_1 \times (1 - (P_2/E_c)^2)^3 \times E_c^{P_3}$ and listed in Table 5.1, here P_2 gives the threshold energy of the corresponding reaction.

In Figure 5.3, the integral cross sections as functions of collision energies E_c (the excitation functions) are displayed for selected $(v,\ j)$ states. The two PESs show a similar behavior which is not surprising since they are very comparable, see section 2.1. For both PESs, the cross sections increase with increasing E_c, which is common for barrier-dominated reactions. Basically, the rovibrational excitation of the OH molecule increases the cross sections for $(v = 0,\ j)$ states. For states with $(v = 1)$, the reagent rotational excitation does not always help the reaction. In particular, the cross sections at lower collision energies (< 0.5 eV) decrease with increasing rotational excitation of OH molecule. This is probably because the increasing rotational quantum number j induces a barrier in the entrance valley of the potential energy surfaces, which will be especially relevant at low collision energies. Note that the errors in our QCT results near the threshold energy are large due to the very low reaction probabilities. In addition, the QCT method does

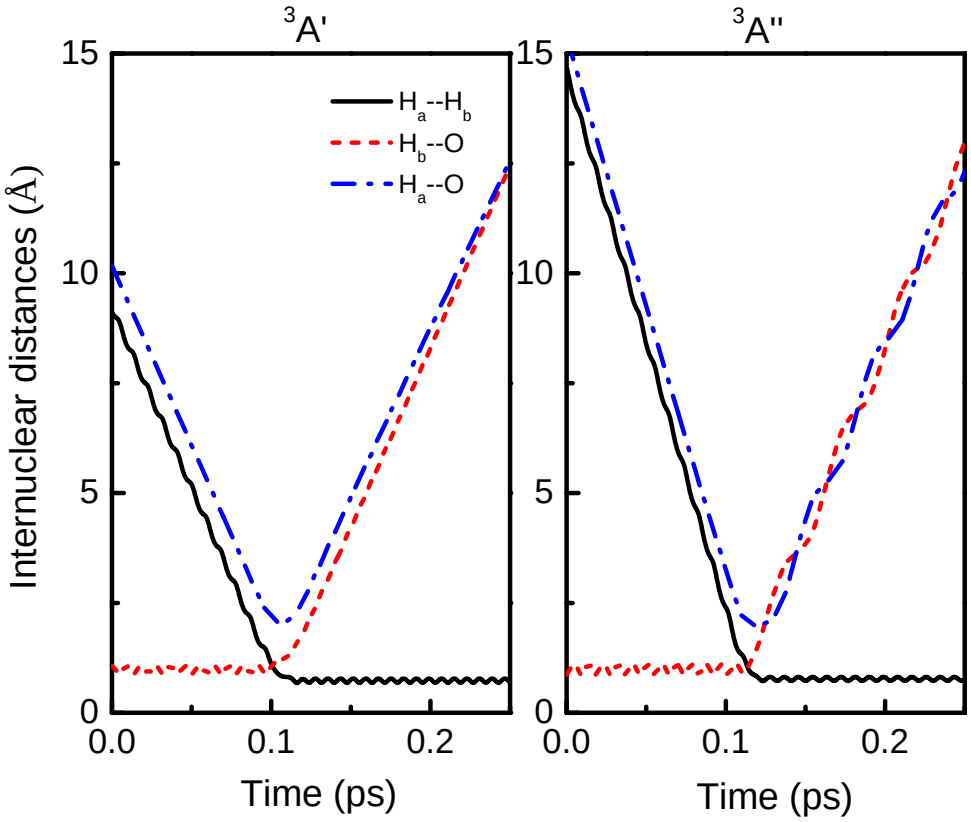

Figure 5.4 — Typical reactive trajectories for the abstraction reaction $H_a + H_bO \longrightarrow O + H_aH_b$ on the $^3A'$ and $^3A''$ PESs, namely internuclear distances of H_aH_b, H_bO and H_aO as functions of propagation time.

not include tunneling which could be important near threshold.

It is seen that the cross sections for different $(v,\ j)$ states are larger for the $^3A''$ PES than for the $^3A'$ surface, indicating that the $^3A''$ surface plays a more important role in the rate constants. The same conclusion was found previously in quantum mechanical investigations of the reverse reaction, O + H_2 in the energy range 0.5 – 1.2 eV (Balakrishnan 2003).

We "observed" a large number of trajectories over the two PESs in every rovibrational state and found that all reactions are dominated by the direct reaction mechanism, that is, the attacking atom H_a collides with the OH_b molecule and forms an H_2 that leaves immediately, indicating that the broad van der Waals well is too shallow to "trap" any atom, even near the threshold collision energy. Some typical trajectories are shown in Figure 5.4.

5.3.2 Rate constants

The specific reaction rates for various $OH(v,\ j)$ states as well as thermal rate constants were derived from the fitted cross sections, and then fitted to the Arrhenius form. By fitting the data separately to two temperature ranges (200 – 1000 K and 1000 – 2500 K) on a logarithmic scale, the fitting errors were significantly reduced compared to the fitting

Table 5.2 — Thermal rate constants fitted to $k(T) = \alpha \times (T/300)^{\beta} \times e^{(-\gamma/T)}$ (cm^3 molecule^{-1} s^{-1}).

	200 – 1000 K			1000 – 2500 K		
$(v,\ j)$	α	β	γ	α	β	γ
(0, 0)	2.32×10^{-16}	1.448	2597	1.60×10^{-11}	0.031	3992
(0, 1)	1.05×10^{-16}	1.557	2621	1.93×10^{-11}	0.012	4114
(0, 2)	1.25×10^{-16}	1.527	2656	1.60×10^{-11}	0.030	4124
(0, 3)	2.42×10^{-16}	1.440	2762	1.83×10^{-11}	0.013	4182
(0, 4)	4.37×10^{-16}	1.374	2881	2.00×10^{-11}	0.010	4227
(0, 5)	1.12×10^{-16}	1.553	2723	2.09×10^{-11}	0.008	4230
(0, 6)	8.32×10^{-17}	1.584	2544	1.35×10^{-11}	0.059	4043
(0, 7)	3.76×10^{-17}	1.669	2105	4.04×10^{-12}	0.200	3582
(0, 8)	8.20×10^{-17}	1.579	2047	5.03×10^{-12}	0.179	3439
(0, 9)	6.30×10^{-17}	1.614	1814	3.01×10^{-12}	0.247	3186
(0, 10)	1.67×10^{-16}	1.514	1914	5.34×10^{-12}	0.197	3225
(0, 11)	1.44×10^{-16}	1.535	1679	3.70×10^{-12}	0.248	2973
(0, 12)	2.45×10^{-16}	1.481	1626	3.96×10^{-12}	0.253	2866
(0, 13)	3.31×10^{-16}	1.447	1647	3.87×10^{-12}	0.260	2845
(0, 14)	9.26×10^{-16}	1.330	1431	3.61×10^{-12}	0.285	2509
(0, 15)	1.93×10^{-15}	1.245	1328	3.67×10^{-12}	0.294	2333
(0, 16)	2.16×10^{-15}	1.233	1148	3.01×10^{-12}	0.324	2127
(1, 0)	1.49×10^{-13}	0.722	307	3.90×10^{-12}	0.312	751
(1, 1)	1.69×10^{-13}	0.711	531	4.82×10^{-12}	0.290	991
(1, 2)	1.44×10^{-13}	0.735	750	6.21×10^{-12}	0.262	1261
(1, 3)	1.55×10^{-13}	0.735	979	1.14×10^{-11}	0.192	1543
(1, 4)	8.03×10^{-14}	0.828	1123	1.43×10^{-11}	0.170	1782
(1, 5)	2.59×10^{-14}	0.973	1064	1.07×10^{-11}	0.207	1816
(1, 6)	1.02×10^{-14}	1.085	883	6.33×10^{-12}	0.268	1693
Thermal	3.53×10^{-18}	2.078	2518	2.78×10^{-11}	0.059	4496

throughout the overall temperature range. The fitted parameters are listed in Table 5.2.

Selected rate constants for various OH($v,\ j$) states as a function of inverse temperature are shown in Figure 5.5. As expected, the rate constants increase with increasing temperature and follow an Arrhenius trend. For both PESs, the vibrational excitation of OH evidently accelerates the reaction. The rotational excitation of OH accelerates the reaction for ($v = 0,\ j$) states except for $j = 0$ on the $^3A'$ PES. For ($v = 1,\ j$) states, similar to the conclusions from the corresponding cross sections, rotational excitation reduces the rate constants due to the induced effective barriers at lower temperatures.

Figure 5.6 compares the calculated rate constants for the ($v = 0,\ j = 0$) level summed over both PESs by the different QCT, TST, CVT, CVT/ZCT, and CVT/SCT methods in the temperature range of 200 – 2500 K. The calculated TST and CVT rate constants are smaller than the QCT results in the temperature range below 500 K, whereas the improved CVT treatments, namely zero-curvature tunneling (ZCT) and small-curvature tunneling (SCT) methods, which attempt to take into account tunneling effects, indeed produce more accurate rate constants for the title reaction. The outcome of the transition state calculations is rather surprising. At low temperatures the TST rate is four orders of magnitude smaller than the QCT rate, but both rates are, due to the ~ 0.5 eV barrier,

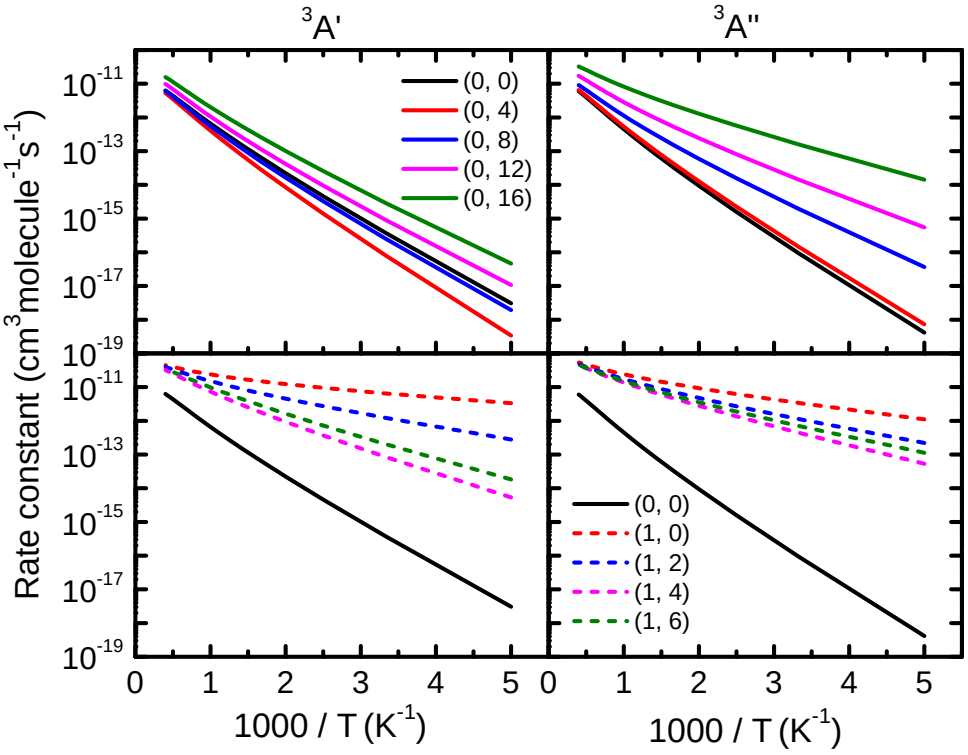

Figure 5.5 — State-resolved rate constants as functions of inverse temperature for individual OH(v, j) levels.

very low anyway. Both methods could at these low temperatures suffer from neglect of tunneling. The standard CVT method produces the same rates as pure TST at the low temperatures, but adding corrections for tunneling according to the SCT formalism makes the CVT/SCT rates agree with the QCT rates. This agreement between the QCT and CVT/SCT results at low temperatures must be largely fortuitous since QCT does not take tunneling into account. The question of the importance of tunneling can only be addressed properly by a full quantum mechanical (QM) calculation of the OH + H reaction rates on the triplet potential energy surfaces. Such calculations have not yet been performed and thus one can only speculate on the basis of results for other atom-diatom exchange reactions with a barrier for which full QM calculations have been performed. In the text book example of such a reaction, the H + D_2 hydrogen/deuterium exchange reaction, as discussed, e.g., in Ju et al. (2009), there is near perfect agreement (within 5% on average) between full QM and QCT rates even at temperatures as low as 200 K, suggesting that for the H + D_2 case tunneling is less important. In that study, also a CVT variant which includes tunneling corrections, named MCPVAG, was found to produce the same rates as were obtained with QCT and QM, while the native TST and CVT gave nearly identical but much lower rates. We therefore conclude that good agreement between QCT and CVT/SCT rates can be reached as found in both our studies and that in Ju et al. (2009), but for reasons that are not yet understood.

Figure 5.7 shows a blow-up of the QCT results in the 200-1000 K range on a linear scale. This figure also includes the previous studies by Tsang & Hampson (1986) whose

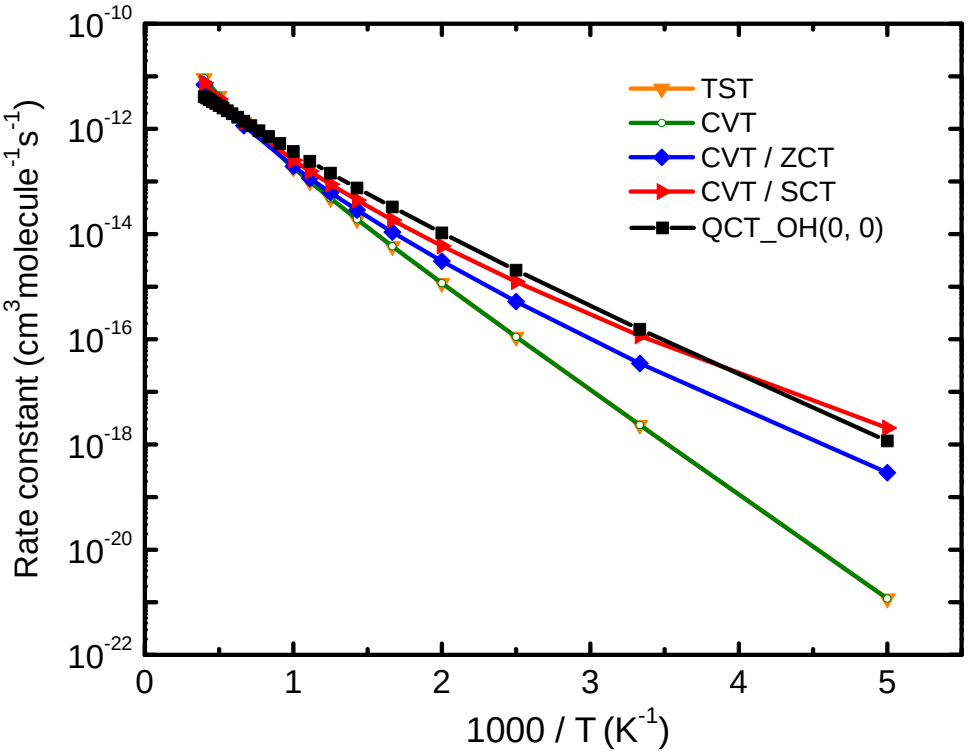

Figure 5.6 — Plot of rate constants for the title reaction with OH in the ($v = 0,\ j = 0$) state, as functions of inverse temperature in the range of 200 – 2500 K, which were calculated from QCT and various TST methods. Both the x- and y-axis are in base 10 logarithmic scales. Rate constants at each electronic state were calculated by considering the results from two PESs, i.e., $({}^3A' + {}^3A'')/3$.

rate constants were derived from the reverse O + H_2 reaction (over the 298 – 2500 K range) that obtained by Walch et al. (1980). The 1986 Tsang *et al.* results are in good agreement with the present thermal QCT results, which were calculated using a more accurate benchmark PESs, with differences typically 50%.

Another interesting phenomenon in Figure 5.7 is that the values of the thermal rate constants are higher than those at ($v = 0,\ j = 0$) state when $T > 600$ K, but lower when $T \sim 200$ K. This is because at higher temperatures, the higher rotational excitation states, ($v = 0,\ j = 3 - 10$), contribute more to the thermal rate constants, as seen in Figure 5.2. The values of the cross sections at those higher j states are significantly higher, especially at higher energies, see Figure 5.3. Therefore, the thermal rates are also higher.

The importance of the state-selective rate constants computed here for astrochemical applications is demonstrated with two examples. In interstellar shocks with kinetic temperatures $T_{\rm kin}$ of 500 – 2000 K, the OH molecules lose their internal energy more rapidly than their translational energy, so the rotational temperature $T_{\rm rot}$ characterizing the OH excitation is much lower than $T_{\rm kin}$. In this case, the state-specific rate constants for $j = 0$ will be lower than the thermal rate constants at high temperatures. The difference is 30% at 1000 K, increasing to 67% at 2000 K. A reverse situation is provided by the warm (few hundred K) surface layers of protoplanetary disks where OH may be produced by Lyman α photodissociation of H_2O in either vibrationally excited and/or highly excited

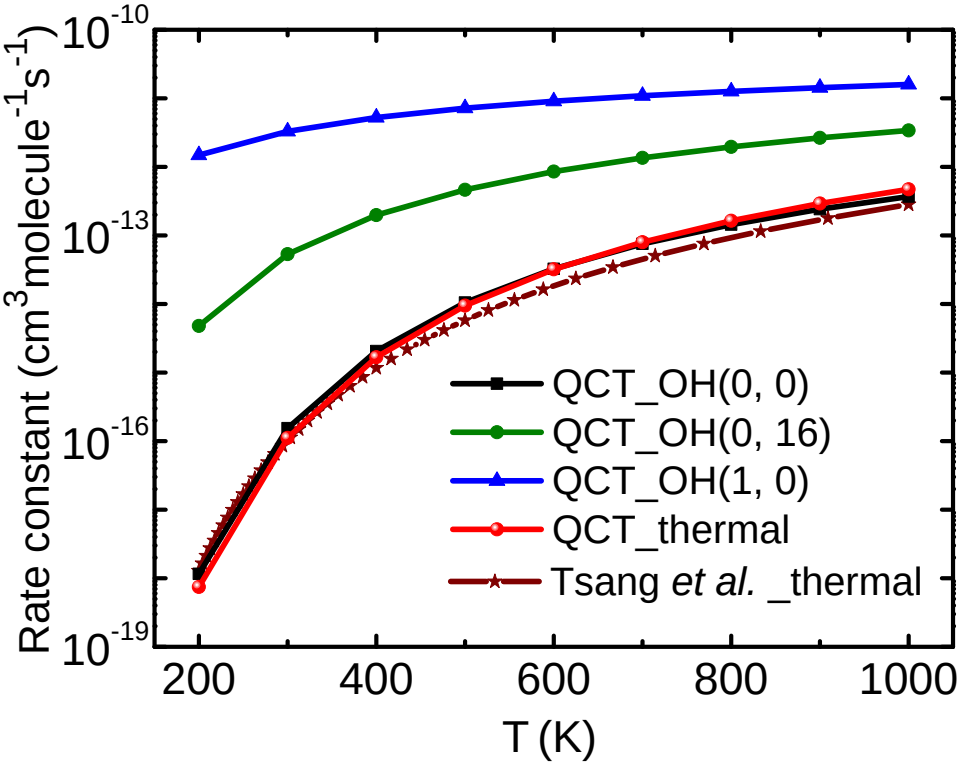

Figure 5.7 — Comparison of the presently calculated thermal rate constants with that of Cohen & Westberg (1983). The figure also illustrates the rotational and vibrational excitation effects on the rate constants. In the plot, x-axis is on a linear scale but the y-axis is on base 10 logarithmic scales. Rate constants for each electronic state were calculated by considering the results from two PESs, i.e., $({}^3A' + {}^3A'')/3$.

rotational levels with values observed up to $j = 35$ (Mandell et al. 2012; Salyk et al. 2008; Pontoppidan et al. 2010). In this case the appropriate rate constants for the OH $(0, j)$ + H reaction are orders of magnitude larger than the thermal ones, as shown in Figure 5.7.

5.4 Concluding remarks

Using accurate *ab initio* PESs, integral cross sections and state-resolved rate constants were calculated for various OH$(v,\ j)$ states for the reaction OH + H $\rightarrow$ O + H_2 and presented in fitted form for temperatures $>$ 200 K. Moreover, thermal rate constants are reported. The reactions occurring on the ${}^3A'$ and ${}^3A''$ PESs are dominated by the direct reaction mechanism, belonging to the abstraction type. The ${}^3A''$ PES plays a more important role in the rate constants at lower temperatures whereas the ${}^3A'$ surface contributes at higher temperatures. Both the rotational and vibrational excitation of the OH molecules will enhance the reaction rates at higher collision energies, but the vibrational excitation has a larger impact than the rotational excitation. In particular, an effective barrier may be induced by the rotational excitation at lower collision energies ($<$ 0.6 eV).

The rate constants presented here should be more accurate than previous values used

in astrochemical models of warm interstellar gas. The state-selective values are found to make orders of magnitude differences compared with thermal ones.

Acknowledgments

X. Li thanks Prof. Keli Han for his continuous encouragement and inspiring advices and Dr. Alan Heays for valuable discussions. The authors thank Drs. Erik Deul and Mark Somers for their assistance. This work is supported by the Dutch astrochemistry network (DAN) from the Netherlands Organization for Scientific Research (NWO) under grant 648.000.002. Astrochemistry in Leiden is also supported by the Netherlands Research School for Astronomy (NOVA), by a NWO Spinoza grant, and by the European Community's Seventh Framework Program FP7/2007-2013 under grant agreement 238258 (LASSIE).